A High-*k* and Low Energy-disorder Spiro-nanopolymer Semiconductor

Dongqing Lin[1], Wenhua Zhang[2], Hang Yin[3], Haixia Hu[3], Chaoyang Dong[1], Yongxia Wang[1], Xinmiao Xie[1,4], Le Wang[1], Hongkai Hu[1], Yongxia Yan[1], Haifeng Ling[1], Jin'an Liu[1], Yue Qian[1], Lei Tang[1], Linghai Xie[1,6]*, Hao Zhang[5], He Zhang[1], Shasha Wang[1], Ying Wei[1]*, Xuefeng Guo[4], Dan Lu[5], Wei Huang[1,6]*

Affiliations:

[1]Centre for Molecular Systems and Organic Devices (CMSOD), Key Laboratory for Organic Electronics and Information Displays & Jiangsu Key Laboratory for Biosensors, Institute of Advanced Materials (IAM), Nanjing University of Posts & Telecommunications, 9 Wenyuan Road, Nanjing 210023, China

[2]National Synchrotron Radiation Laboratory, Anhui Provincial Engineering Laboratory of Advanced Functional Polymer Film, CAS Key Laboratory of Soft Matter Chemistry, University of Science and Technology of China, Hefei 230026, China

[3]School of Physics, State Key Laboratory of Crystal Materials, Shandong University, Jinan, Shandong 250100, P. R. China

[4]Beijing National Laboratory for Molecular Sciences, State Key Laboratory for Structural Chemistry of Unstable and Stable Species, College of Chemistry and Molecular Engineering, Peking University, Beijing 100871, China

[5]State Key Laboratory of Supramolecular Structure and Materials, College of Chemistry, Jilin University, 2699 Qianjin Avenue, Changchun, 130012, China

[6]Frontiers Science Center for Flexible Electronics (FSCFE), MIIT Key Laboratory of Flexible Electronics (KLoFE), Shaanxi Key Laboratory of Flexible Electronics, Xi'an Key Laboratory of Flexible Electronics, Xi'an Key Laboratory of Biomedical Materials & Engineering, Xi'an Institute of Flexible Electronics, Institute of Flexible Electronics (IFE), Northwestern Polytechnical University, Xi'an 710072, Shaanxi, China

*Correspondence to: iamlhxie@njupt.edu.cn; iamywei@njupt.edu.cn; provost@nwpu.edu.cn

Abstract: Ultralow energy disorder integrated with high dielectric constant is fundamental for plastic electronic materials to enhance carrier mobility and potentially afford inorganics-like optoelectronic properties toward the intelligent semiconductors. Herein, we reported the ultralong persistence length ($l_p \approx 41$ nm) effect of organic nanopolymers on exciton and charge carrier behaviors. The state-of-the-art nanopolyspirogrid (NPSG) is synthesized via the spiro-polygridization of A_2B_2-type nanosynthons. The π-interrupted NPSG exhibits an amorphous state with a hole mobility of 3.94×10^{-3} cm^2 V^{-1} s^{-1} and an ultralow energy disorder (<50 meV), to our best knowledge, which surpasses most of the amorphous π-conjugated polymers. Meanwhile, the high dielectric constant (k = 8.43) of NPSG is also observed that probably is attributed to the dipole polarization enhancement from locking spiro-polygridization effect. The covalent nanoscale ordering of NPSG-based nanopolymers is promising to overcome molecular limitaion for organic photovoltaics and nanoelectronics.

Introduction

Organic materials hold promising advantages of the fourth-generation semiconductors that would revolute the function and morphology of devices and integration circuits toward flexible electronic intelligence, beyond the Moore's law[1]. Even achieving significant development in light-emitting diodes[2], photovoltaics[3] and transistors[4], organic multifunctional semiconductors still suffer from severe challenges such as low carrier mobility (μ < 10^{-3} cm^2 V^{-1} s^{-1} in amorphous state)[5] and low dielectric constant (k = 2~4)[6], versus hybrid perovskites[7] with μ > 100 cm^2 V^{-1} s^{-1} and k = 28~60. The central mission is to innovate polymer semiconductors with inorganics-like optoelectronic properties, including the band-like carrier transport[8] and Wannier-Mott-like excitons[9] under high dielectric constant[10]. Essentially, the defficiency of molecular scale effects[11] (limited in shorter than 10 nm) is mainly responsible for poor optoelectronic performance. Nanoscale ordering features with little trapping defects[12] is the prerequisite of efficient polarization behaviors. Although energy disorder is reduced via noncovalent nanoscale semi-crystalline strategies[13,14], there is no significant improvement on intrinsically amorphous polymers that generally exhibit the incompatible contradiction between high dielectric constant and low energy disorder[15,16]. As a central toolbox of the cross-scale chemistry, gridization strategy enable to potentially extend the maximum persistence length (l_p) beyond ~100 nm and transform molecular π-backbone into covalently ordered nanoarchitectures with sizes of 10~100 nm, by means of its vertexes' extensibility, expandability, scalability and programmability[17]. Futhermore, different from graphene nanoribbons[18], ladder polymers[19,20] and other covalently one-dimensional nanoobjects[21-23], organic nanopolymers with gridon-based repeat nano-units principally possess the dual merits of both polymers and CNT/graphene-like nanocarbons[24]. However, organic nanopolymers with the single bond linkage, recorded[25] in the l_p of 16 nm, is not long enough to challenge over covalent nanoscale ordering effects on integrating ultralow energy disorder with high-k feature that are bottleneck in the potential application of plastic/flexible/nano electronics[21,26,27].

To increase l_p scale, the conformational entropy of organic nanopolymers should be reduced via the covalent/noncovalent lock of electroactive linkage[28] between nanogrid repeat units. Distinct from ladder-type square nanogrids with two arms extended in mutually parallel direction[29], an alternative installing paradigm is the rhombus-type polygrid (RPG) that consists of rhombus-type gridarene nanounits (RGs) extended in diagonal direction via sharing the nanogrid vertexes[17]. This kind of RPGs is similar to the shapes of macroscopically expandable coat & cap racks and can be also found in scissor lifts and window lattices (Fig. 1a). Furthermore, such RPG backbone can be separated into two independent single chains. In terms of double-chain feature, RPGs are analogous to double-strand DNA[30] with l_p = 53 nm, far longer than that of the single-stranded counterpart (l_p = 1.5 nm). Accordingly, RPGs are expected to have an extraordinarily long l_p property through synergistically double-bond-linked polygridization effects. Herein, we introduce the four-armed linkage of orthogonal spiroarenes (as diagonal vertexes of RGs) to perfectly create one kind of double-stranded nanopolymers, nanopolyspirogrids (NPSGs, Fig. 1b). In addition, the target NPSG consists of wide-bandgap blue-emitting terfluorenyl moieties, which serve as longitudinal girders that are covalently fixed by 3,3-dithiophenyl transverse beams at the spiro-positions (Fig. 1c). The dithiophenyl groups are selected mainly because of their regular linkage and high-efficient Friedel-Crafts

welding reaction[31]. As a result, we successfully synthesize spirodithiophenefluorene (SDTF)-based spirodigrid (SDGs) and one-dimensional NPSGs with a length × width × height scale of 2~50 × 2 × 2.5~3.5 nm^3, through the kinetically controlled spiro-polygridization of A_2B_2-type nanosynthons. The obtained NPSG possesses an ultralong l_p = 41 nm, confirmed by the synchrotron radiation small angle X-ray (SAXS) and static light-scattering (SLS). Further, even with π-interrupted backbones in amorphous states and wide-bandgap properties, ultrarigid NPSG surprisingly achieves higher dielectric constant and carrier mobility than general π-conjugated polymers, along with the ultralow energy disorder falling in the semicrystalline level, which is consistent with our design of covalent nanoscale ordering.

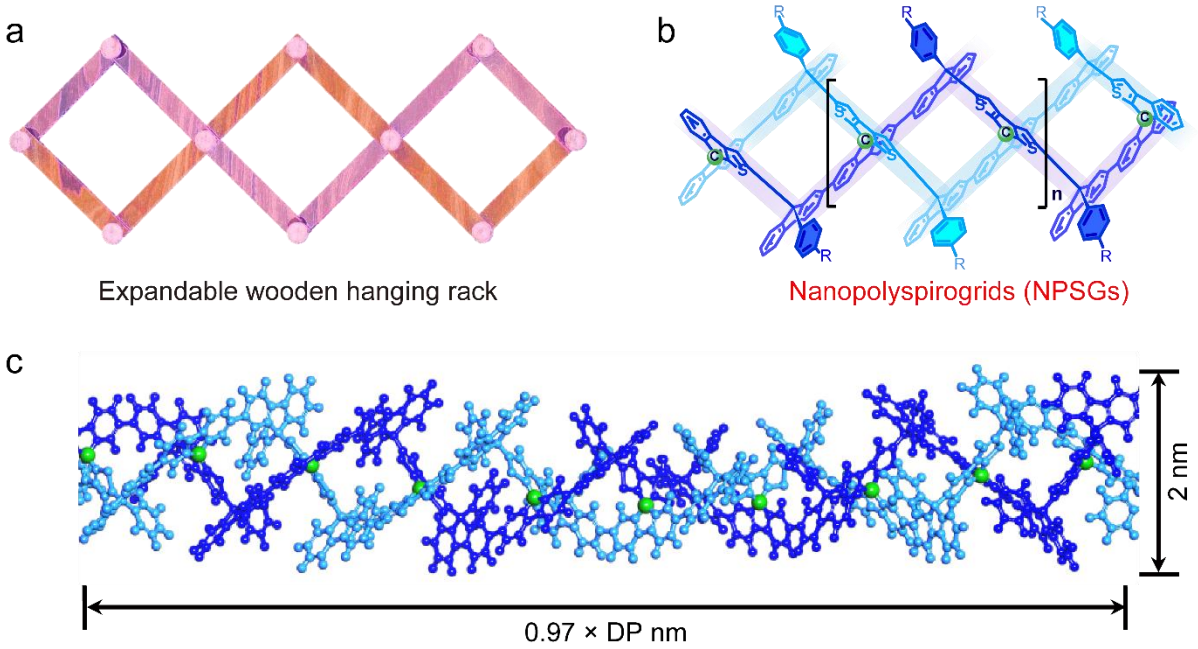

Fig. 1 | Structures and theoretical rigidity of nanopolyspirogrids (NPSGs). (a) A wooden structure of expandable hanging rack. (b) Molecular structures of NPSG. (c) The 3D atomistic models of NPSG nano-architecture segments.

Results and discussion

Synthesis and characterizations of NPSG nanochains

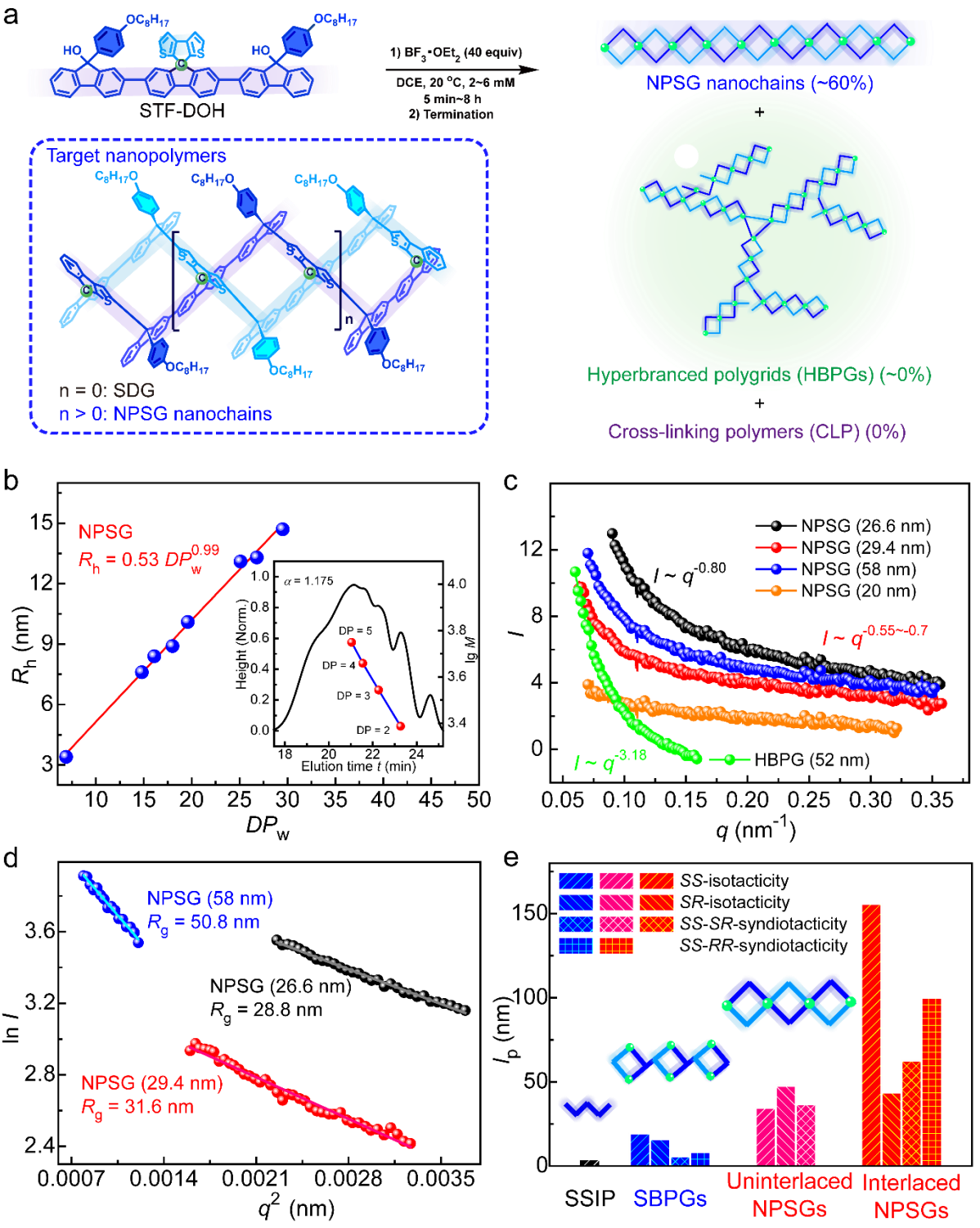

Fig. 2 | Synthesis and characterizations of NPSG. (a) Chemical equation of polygridization reaction. The likely structure of hyperbranched polygrid (HBPG), as byproducts, is provided in Supplementary Fig. 19. (b) The R_h relying on DP_w. The calibration of NPSG oligomers (DP = 2~5) from GPC spectra was also provided to calculate the Mark-Houwink exponent (α). (c)

The scaling plots $I \sim q^{-d}$ of NPSG and HBPG. The average contour length of NPSG (in the brackets) were transformed from individual R_h or DP_w values. (d) The Quinier plots of NPSG with various contour length (marked in the brackets). The calculated radius of gyration (R_g) were also provided. (e) The simulation of l_p of SSIP (orange), SBPGs (deep blue) and NPSGs (pink and red). The SSIP chain is defined as the single-chain of NPSG that removes all spiro-carbon atoms.

NPSGs can be synthesized via the Friedel-Crafts polygridization of A_2B_2-type SDTF-based terfluorenyl diol (STF-DOH) nanosynthon, which consists of a pair of 3,3-bithiophene-type benzenoid (B) groups at the middle and two tertiary alcohols (A) at the ends. The polygridization of STF-DOH was conducted smoothly under the condition of $BF_3{\cdot}OEt_2$ (as acid catalyst) in 1,2-dichloroethane (DCE) solvent[31] (Fig. 2a). The linear soluble NPSG is afforded in ~60% yield when the concentration of STF-DOH ($C_{STF\text{-}DOH}$) is 2 mM. Further, elongating the reaction time from 0.5 min to 4~8 h leads to the increase in the number-average degree of polymerization (DP_n) of NPSG from 5.2 to 26.1 (Supplementary Fig. 9), corresponding to the average contour length (l_c) of 25~30 nm. However, the longer polygridization time (13~22 h) results in the formation of hyperbranched polygrids (HBPGs, in Supplementary Fig. 10) rather than longer NPSG nanochains, which suggests the kinetic control feature of spiro-polygridization. To obtain longer NPSG, we increased $C_{STF\text{-}DOH}$ to 6 mM and obtained NPSG with the chain length of ~58 nm, with the approximate weight-average degree of polymerization (DP_w) of ~65 (Supplementary Fig. 11). Further elevating $C_{STF\text{-}DOH}$ to 12~16 mM affords insoluble cross-linked polymers (CLP) in ~90% yield, whereas NPSG nanochains are not obtained.

The linear structural features of NPSG with the length of 2~50 nm were characterized by nuclear magnetic resonance (NMR), Fourier transform infrared (FT-IR), gel permeation chromatography (GPC), dynamic light scattering (DLS) and SAXS. According to ^{13}C NMR spectra (Supplementary Fig. 28), the nonexistence of carbon signals at 54 ppm (the 9-position of phenylfluorenes) and 83.4 ppm (the 9-position of fluorenols) supports the occurrence of polygridization and the termination with A_1B_1 synthons, which eliminate hydroxyl groups at chain-ends (also confirmed by FT-IR spectra in Supplementary Fig. 29). Further, the Mark-Houwink exponent (α) of NPSG oligomers was calculated to be 1.175 from GPC spectra (Fig. 2b), which falls into the range of rod-like conformation[32] in α = 1.0~1.7. Meanwhile, the relationship $R_h \sim DP_w^{0.99}$ from DLS characterization also reveals the rod-like conformation of NPSG with DP_w = 15~30 and R_h = 7.6~14.7 nm, consistent with the visualization of atomic force microscopy (Supplementary Fig. 32). Via SAXS characterization, rod-like NPSG nanochains are verified by the nonexistence of intrachain folding in Kratky plots q^2I and the ultralow mass fractal dimension from scattering laws $I \sim q^{-0.8\sim-0.55}$, distinct from HBPG with $I \sim q^{-3.18}$ features (Fig. 2c and Supplementary Fig. 33), where I and q are scattering intensity and scattering vectors, respectively. Deeply, the distance distribution function $P(r)$ of NPSG exhibits a series of peaks at r = 2, 7.5, 12.5 and 18 nm (Supplementary Fig. 35), which indicate the covalently ordered periodic distribution of polygrid segments, distinguished from only a broad Gaussian-like $P(r)$ in random coils[33].

The rigidity of NPSG nanochains was investigated via SLS and SAXS characterizations, as well as molecular dynamic simulations. We obtained the radius of gyration (R_g) of 28.5~31.1

nm for the synthesized NPSG with l_c = 26~30 nm (Fig. 2d), probably indicating $l_p \geq 30$ nm. For longer NPSG nanochains with $l_c \approx 58$ nm, we obtained R_g = 53.2 nm from SLS results and R_g = 50.8 nm from SAXS data (Supplementary Fig. 39). Based on the rigidity calculation[34], the average R_g = 52 nm and l_c = 58 nm afford $l_p \approx 41$ nm, as beyond all soluble π-conjugated polymers[34,35] (l_p =3~20 nm, Supplementary Fig. 41).

Molecular dynamic simulation was further conducted to investigate the effect of spiro-polygridization on the l_p scale (Fig. 2e). Considering various configurations, we evaluated l_p of all NPSG backbones in an approximate Θ state, including interlace-*SS*-isotacticity (l_p = 155.8 nm), interlace-*SR*-isotacticity (l_p = 43.7 nm), interalace-*SS*-*SR*-syndiotacticity (l_p = 62.5 nm) and interlace-*SS*-*RR*-syndiotacticity (l_p = 100 nm), along with uninterlace counterparts (l_p = 34.5~47.6 nm). The backbone rigidity of NPSGs possesses 1.8~27 times higher than that of single-bond-linked polygrids (SBPG) with l_p = 5.7~19.4 nm, consistent with the double-bond-linked spiro-polygridization effect on restricting conformational rotations of RG units (Supplementary Figure 45). Further, l_p of NPSGs are 11~53 times longer than that of single-stranded π-interrupted polymers (SSIP) with l_p = 3.7 nm, which can easily form coil-like conformations. Hence, such DNA-like spiro-polygridization effect diminishes the conformational entropy of NPSG nanochains, which is the prerequisite for enhancing backbone stiffness and transforming coil-like disorder states into covalent nanoscale ordering properties.

Excitonic and carrier behaviors of NPSG

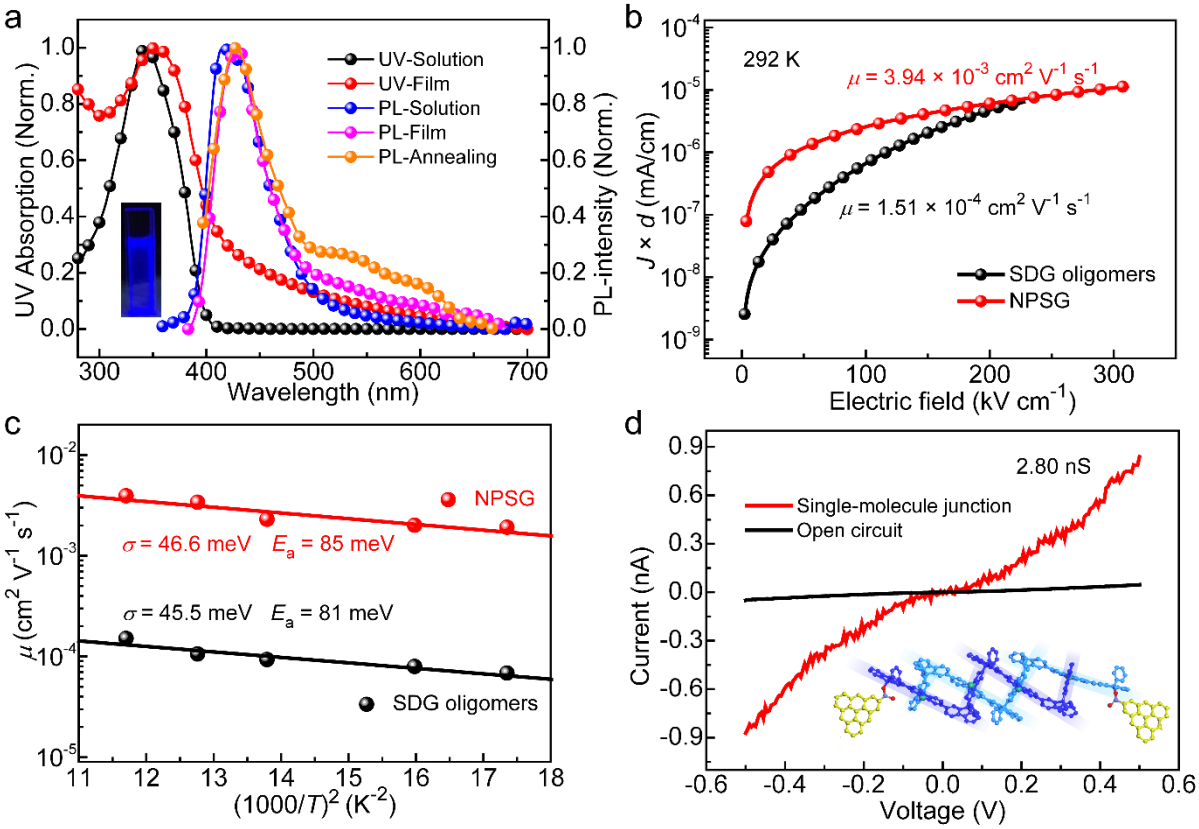

Fig. 3 | Optoelectronic features and carrier mobiliy of NPSG. (a) UV-vis absorbance and PL spectra of NPSG in solution ($CHCl_3$ solvent), pristine and annealing film. (b) The space-charge limit current density (*J*) of NPSG (red) and SDG (black) at 292 K, along with their hole

mobility. The *d* is the thickness of the film. (c) The dependence of temperature on hole mobility for NPSG (red) and SDG (black), along with the energy disorder (σ) and activation energy (E_a). (d) Current-voltage curves of single-chain NPSG and single-molecular devices.

To examine the effect of ultralong l_p feature and covalently large scale on the optoelectronic behaviors of NPSG ($DP_n \approx 26$), we conducted a series of measurements such as ultraviolet-visual absorption (UV), photoluminescence (PL), carrier mobility, and single-molecular conductance.

For UV spectra in solution (Fig. 3a), NPSG nanochains have an absorption peak at 343 nm and a wide shoulder peak at 368~370 nm. Although with an efficient π-conjugation length on terfluorene backbones, NPSG possesses an optical bandgap (E_g) of ~3.11 eV that is almost equivalent to that of tetrafluorene moieties[24] (E_g = 3.10 eV). Moreover, even on π-interrupted backbones, E_g is still gradually decreased from 3.33 eV to 3.11 eV (Supplementary Fig. 53) when increasing the nanochains length from SDG (~2 nm) to NPSG (> 20 nm). These results indicate that π-interrupted NPSG still enables to enhance delocalized excitonic behaviors, probably associated with the covalently large scale effect. For PL spectra in solution, NPSG possesses an deep-blue emission at 415 nm with a lifetime of ~1.07 ns (Supplementary Fig. 54) and a larger Stokes shift of ~68 nm, totally different from ladder-type polymers with small Stokes shifts of 5~25 nm.[36] On the film, NPSG maintains the blue emission at ~430 nm without the obvious g-band defect emission, even after annealing under 260 ^{o}C temperature and air atmosphere (Supplementary Fig. 55). Thus, NPSG-based wide-bandgap materials enable to compete with polyfluorenes[37,38], ZnO nanoparticles[39] and CNT (without emission)[40].

The carrier mobility of amorphous NPSG film was investigated via space-charge limited current (SCLC) method. Under the temperature of 292 K (Fig. 3b), NPSG exhibits an outstanding zero-field hole mobility (μ) of 3.94×10^{-3} cm^2 V^{-1} s^{-1}. To our best knowledge, such hole mobility is the highest value (Supplementary Fig. 58) among all fully π-interrupted molecules[41] with $\mu = 10^{-7}$~10^{-4} cm^2 V^{-1} s^{-1}. Especially, it is unexpected that the hole mobility of π-interrupted NPSG can be even higher than that of amorphous π-conjugated polymers including polythiophenes[42] (in amorphous state, $\mu \approx 1 \times 10^{-3}$ cm^2 V^{-1} s^{-1}) and polyfluorenes[43,44] (in amorphous state, $\mu \approx 10^{-7}$~10^{-5} cm^2 V^{-1} s^{-1}). In contrast, amorphous SDG oligomers exhibit an evidently lower current density under the same electric filed, and possessed a mobility $\mu = 1.51 \times 10^{-4}$ cm^2 V^{-1} s^{-1}, as an order of magnitude lower than that of NPSG. These results support the covalently large scale effect on improving charge transport, which was always hidden by the effective conjugated length effect and was effectively diminished by the short persistence length effect in conventional organic semiconductors[10].

Further, we studied the temperature-dependent carrier mobility, energy disorder and activation energy of amorphous NPSG film to uncover the physical mechanism during carrier transport. In Fig. 3c, even under low temperature 240 K, NPSG still displays a high carrier mobility of $\mu = 1.93 \times 10^{-3}$ cm^2 V^{-1} S^{-1}, which indicates the relatively weak temperature-dependence on hole transport. According to the Gaussian disorder model[45], NPSG displays an ultralow energy disorder (σ) of 46.6 meV, which is far lower than that of amorphous π-conjugated polymers (Supplementary Fig. 60) with obviously shorter l_p, including polyfluorenes[43] with $\sigma \approx 100$ meV and $l_p \approx 6$~9 nm, poly-*p*-phenylene vinylenes[46] with $\sigma \approx 160$ meV and $l_p \approx 7$ nm, as well as polythiophenes[42,45] with $\sigma \approx 70$ meV and $l_p \approx 3$~10 nm.

Meanwhile, the activation energy (E_a) of amorphous NPSG film is 85 meV that can even fall into the semicrystalline range[5] of polythiophene with E_a = 50~100 meV, as lower than other amorphous conjugated polymers[5] with E_a = 150~250 meV. These results confirm the ultralong l_p scale effect that efficiently suppresses the defect scattering and trapping levels to decrease the width of density-of-states (DOS). Deeply, through quantum calculation (Supplementary Fig. 61-63), the highest occupied molecular orbital (HOMO) and its degenerated orbital levels for hole transport are distributed on both dithiophenyl and monofluorenyl planes of STDF moieties, which should be arranged in covalently well-ordered states according to the narrow DOS feature. In addition, the ultralow energy disorder is similarly observed in SDG oligomers (σ = 45.5 meV and E_a = 81 meV), which confirms the theoretical observation of gridization effect on lowering reorganization energy[47]. The above results also reflect the ultrastiff NPSG nanochain with maintaining little conformational defects.

The single-molecular diode device was also applied to investigate the conductance (G) of a NPSG nanochain with the length of 15~20 nm. In Fig. 3d, NPSG nanochain exhibits an approximately symmetric current (I)-voltage (V) curve, consistent with the typical diode feature. The conductance was enhanced when increasing the bias from 0 to 0.5 V. The highest conductance of NPSG was up to G = 2.8 nS, although such conductance is far lower than that of fully π-conjugated molecules[21] with $G \approx 10^{-7}$~10^{-5} S (in the length of 2~5 nm length). Nevertheless, the intrisincally low conductance of NPSG naonchain probably originates from its π-interrupted backbone, which suggests a potential candidate for the semiconductive molecualr nanoelectroncis.

Dielectric properties and polarization mechanism

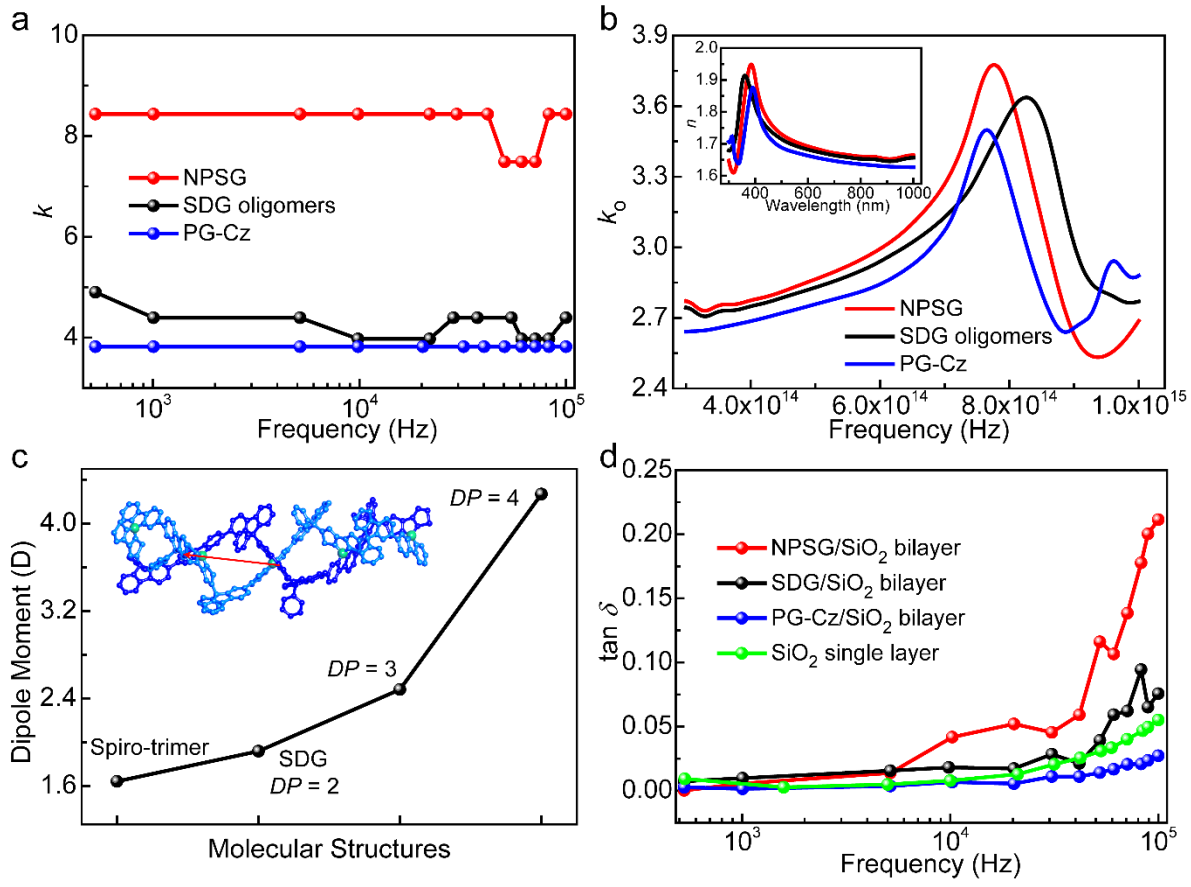

Fig. 4 | **Dielectric features of NPSG.** (a) The dielectric constant (k) in the frequency range of 500~10^5 Hz. (b) The optical dielectric constant (k_o) and refractive index (n) of NPSG and other nanopolymer films. (c) The dependence of DP on the dipole moment, via quantum calculations. The dipole direction on the NPSG oligomer (DP = 4) was marked in red arrow. (d) The dielectric loss tangent (tan δ) of nanopolymer/SiO_2 bilayer at 500~10^5 Hz.

The dramatic spiro-polygridization effects on the dielectric constant (k) were unexpectedly observed at the frequency scope of 10^3~10^5 Hz (Fig. 4a), via impedance analyzer. We found that NPSG had an obviously higher $k \approx 8.43$ than that of single-bond-linked polygrid PG-Cz ($k \approx 3.82$), as well as ungridized π-conjugated polythiophenes[6] ($k \approx 3.75$) and polyfluorenes[48] ($k \approx 2.75$). Thus, even in the absence of cyano or sulfone groups with large dipole moments[6] of 4.0~4.3 D, such spiro-polygridization effect still ingeniously enhances the polarization behaviors for high-k properties. This feature of NPSG is completely distinguished from the porous effect of covalent organic frameworks[49] that reduces k value to 1.2~1.6 through large free volume. Further, SDG oligomers exhibit the relatively lower dielectric constant of $k \approx 4.39$. These results indicate that the covalently large scale effect also supports the high-k feature, which is consistent with the delocalized excitonic behavior, the less electric field-dependent current density (Fig. 3b), and the high mobility of NPSG, probably owing to more efficient charge screening[50] for lower excitonic binding energy[10].

We investigated the polarization enhancement mechanism of spiro-polygridization effect. Considering the frequency scope of 10^3~10^5 Hz, the high-k feature of NPSG likely originates from the electronic and atomic polarization, as well as the dipole polarization. The optical dielectric constant (k_o) were tested to uncover the contribution of electronic and atomic polarization. At the high frequency of $3 \times 10^{14} \sim 7 \times 10^{14}$ Hz, the refractive index (n) of 1.66~1.81 and the extinction coefficient (K) of 0~0.008 are transformed into k_o = 2.77~3.27 for NPSG film (Fig. 4b), as comparable to SDG oligomers (n = 1.77~1.66 and k_o = 2.74~3.13) and PG-Cz (n = 1.75~1.63 and k_o = 2.64~3.08). The difference between k_o at high frequency and k at low frequency was obviously observed in polygrid backbones, especially for NPSG with k - k_o = 5.16~5.66, which is distinct from π-conjugated polyfluorenes[51] ($n \approx 1.6$ and $k_o \approx 2.5$) and polythiophenes[52] ($n \approx 1.92$ and $k_o \approx 3.6$) with $k \approx k_o$. These results rule out the significant enhancement of electronic and atomic polarization from the spiro-polygridization effect. Thus, we deduced that the dipole polarization should be effectively strengthened by spiro-polygridized nanochains.

The theoretical calculations of dipole moment (Fig. 4c) were further analyzed to confirm the enhancement of dipole polarization. We discovered that the longer NPSG backbones have higher dipole moment, from 1.643 D (ungridized spiro-trimer), 1.919 D (SDG), 2.482 D (DP = 3 of NPSG oligomers) to 4.269 D (DP = 4 of NPSG oligomers). The dipole direction is roughly along the NPSG main-chain. On the prerequisite of ultralong l_p property, the dipole direction with enhancing dipole moment can be sustained when increasing the length of rod-like NPSG nanochain, which is consistent with more efficient dipole polarization from covalently large scale effect. It is noted that such dipole polarization enhancement for high-k feature can be perfectly integrated with ultralow energy disorder, which is rather difficult to realize in other high-k organic polymers via adding polar groups on flexible alkyl chains[6,15]. As screening coulombic attraction between charges mainly relies on the static dielectric

constant from efficient dipole polarization[53], high-*k*-based NPSG offers a potential approach to design advanced hole-transport materials in the application of OPVs[50].

Finally, we investigated the spiro-polygridization effect on the dielectric loss tangent (tan δ) of nanopolymer/SiO_2 bilayer. In Fig. 4d, the NPSG/SiO_2 bilayer possesses tan δ = 0.05~0.20 at 10^4~10^5 Hz, which are obviously higher than that of the single SiO_2 layer with tan δ = 0.008~0.055, the SDG/SiO_2 bilayer with tan δ = 0.02~0.08, the PG-Cz/SiO_2 bilayer with tan δ = 0.006~0.027 and polyfluorene/SiO_2 bilayer with tan δ = 0.01~0.03 (Supplementary Fig. 75). These results suggest that adding NPSG layer obviously increases the leakage current and affords higher conductivity for dielectric layers[54], contrary to the decreased leakage current when adding PG-Cz or polyfluorene layer. The conductivity enhancement from spiro-polygridization effect is also consistent with the high-*k* feature of NPSG.

Discussion

In summary, we create an ultrarigid spiro-nanopolymer with the ultralow energy disorder and high dielectric constant, through the covalent nanoscale ordering modulation of spiro-polygridization effect. This kind of polygridization strategies reduces the conformational entropy and then increases the main-chain rigidity to $l_p \approx 41$ nm, resulting in hybridized intermediate between organic polymers and CNTs. Further, the conformational defects and trapping levels were suppressed to induce covalently large scale effect, which gives an excellent hole mobility (μ = 3.94 × 10^{-3} cm^2 V^{-1} s^{-1}). Meanwhile, the dipole polarization is enhanced with higher dielectric constant (k = 8.43) and conductivity. To our best knowledge, these results surpass most of the amorphous π-conjugated polymers reported in the literatures. Our polygridization strategy probably become the state-of-the-art cross-scale chemistry to hierarchically modulate the persistence length and optoelectronic behaviors of organic nanopolymers and to challenge the record semiconducting device performance. By means of such polygridization-type molecular integration technology (MIT), organic nanopolymer semiconductors would become the potential candidates of the fourth-generation semiconductors with the feature of high-performance, multifunctionality, intelligence as well as ubiquity to fulfill the requirement of flexible/nano electronics and organic intelligence.

Methods

Materials. The detailed synthetic procedures of substrate synthons and NPSG chains are described in the Supplementary Information files.

Gel permeation chromatography (GPC). The GPC characteristics were conducted on a HP1100 HPLC system possessing 7911GP-502 and GPC columns using polystyrenes as the standard and tetrahydrofuran (THF) as the eluent at a flow rate of 1.0 mL/min at 25 ^oC. The concentrations of NPSG solutions were about 0.8 mg/ml.

Dynamic Light Scattering (DLS) and Static Light Scattering (SLS). The DLS characterizations of NPSG solution ($CHCl_3$ as a solvent) were determined by a Brookhaven instrument (ZetaPALS) to obtain R_h. The operating wavelength of light source is 632.8 nm. The SLS measurements were performed to calculate R_g, via ALV/CGS-3 light-scattering

spectrometer that is equipped with an ALV/LSE-7004 multiple-τ digital correlator. All of the operating wavelength are 632.8 nm for light source.

Small-angel X-ray Scattering (SAXS). The scattering datum were provided via the synchrotron radiation SAXS from Shanghai Synchrotron Radiation Facility. The distance from the sample cell (with mica windows in the path length of 1.5 mm) to the detector was 1 m. The wavelength of X-ray was 1.2 Å. The collected scattering vectors q ranges from 0.01 to 0.4 nm. The substrate of the solvent (toluene) from the solution scattering was performed before the analysis. The data were collected with the exposure time of 2 s, the acquired period of 2.01 s, and the images of 10. The measured NPSG solutions were 0.5~2 mg/ml in toluene solvents.

Molecular dynamic simulations. The molecular models of NPSG-based spirotrigrids were constructed and calculated via the Forcite plus module in the software Material Studio. The geometry optimization were performed based on the SMART algorithm (as the cascade Steepest Descent-ABNR-Quasi-Newton algorithm). The simulations of conformational motions of spirotrigrids were based on the NVT ensemble (in vacuum), the pcff forcefield, the time-step of 0.2 fs and the total time of 100 ps.

Ultraviolet-Visual absorption (UV-Vis) and Photoluminescence spectra (PL). The solution was prepared under the concentration of 10^{-2} mg/ml in $CHCl_3$ or DCE solvent. The film was spin-coated from the solution (DCE solvent, the concentration of 8 mg/ml) under the 800 rad/s. The UV spectra (LAMBDA 35) were used to characterize the photophysical properties of their ground states. The PL spectra (RF-6000 Plus) were obtained to study the excitonic behaviors of their excited states.

Measurement of space-charged-limited current for carrier mobility (μ). The hole-only device with the structure of ITO/PEDOT:PSS/NPSG/Au was fabricated according to the literature[46]. The poly(3,4-ethylenedioxythiophene)-doped poly(styrene sulfonic acid) (PEDOT:PSS) layer and NPSG layer (or SDG oligomers, both in chlorobenzene solvent) were prepared via spin-coating at the spin rate 7000 RPM and annealing under 140 °C (10 min). For the space-charged-limited current measurement, injecting the charge carriers into the thin-film active layer was performed under the DC voltage, through a source measure unit (SMU) Keithley (Model 2612B) that also record the currents under different voltage conditions. The energy disorder (σ) was calculated via the equation $\mu\ (T) = \mu_\infty \exp\ [-(2\sigma/3k_BT)^2]$, where μ_∞, k_B and T are defined as the carrier mobility at ultrahigh temperature, the Boltzmann constant and the temperature, respectively. The activation energy (E_a) of carrier transport was calculated via the equation $\mu\ (T) = \mu_\infty \exp\ (-E_a/k_BT)$.

Single-molecular electronic device. A new dash-line lithographic (DLL) method, referred to the literature[53], was used to fabricate the single-molecular electronic device. For the linkage of a polymeric single-chain via ester linkage, NPSG were dissolved in dichloromethane with the concentration ~10^{-4} M, followed by adding graphene devices and carbodiimide dehydrating/activating agent. After 2 days, the NPSG device was taken out from solution. Such device was washed through copious acetone and ultrapure water solvent, and then was dried

under N_2 atmosphere. We used an Agilent 4155C semiconductor characterization system and a Karl Suss (PM5) manual probe station to measure the current (I)-voltage (V) curve under the ambient atmosphere.

The calculation of dielectric constant (*k*) of NPSG. The diode device structure Cu/SiO_2/NPSG/Si (n^+) was fabricated to measure the total capacitance C_i, which is transformed to k via the equation $\varepsilon_0/C_i = d_s/k_s - d/k$, where d_s and k_s, ε_0 are defined as the layer thickness, the dielectric constant[8] of SiO_2 (k_s = 3.9) and the permittivity of vacuum (8.85×10^{-12} F/m), respectively. The NPSG layer (from the DCE solution with the NPSG concentration of 5 mg/ml) was spin-coated on the SiO_2 layer, which is followed by annealing under the conditions of vacuum environment, 80 ℃ and 30 min. The procedure and conditions of spin-coating other polymer/oligomer films were the same as those of NPSG. C_i was measured via an impedance analyzer (IM3533), through a frequency sweep of 50~100000 Hz and a bias of 0.1 V. The thicknesses of the NPSG film was measured by an ellipsometry (J.A. Woollam RC2). The dielectric loss (tan δ) of NPSG-based diode device (bilayer of NPSG and SiO_2) was afforded via impedance analyzer a at 10^3~10^5 Hz. The optical dielectric constant (k_o) of NPSG, in the high frequency range of $3 \times 10^{14} \sim 8 \times 10^{14}$ Hz, was calculated via the equation $k_o = n^2 - K^2$, where n and K are defined as the refractive index and the extinction coefficient, respectively. Both were afforded via the ellipsometry characterization.

References

1 Xie, L. H., et al. Polyfluorene-based semiconductors combined with various periodic table elements for organic electronics. *Prog. Polym. Sci.* **37**, 1192-1264 (2012).

2 Wu, T. L. *et al.* Diboron compound-based organic light-emitting diodes with high efficiency and reduced efficiency roll-off. *Nat. Photonics* **12**, 235-240 (2018).

3 Meng, L. *et al.* Organic and solution-processed tandem solar cells with 17.3% efficiency. *Science* **361**, 1094-1098 (2018).

4 Dong, H. *et al.* 25th anniversary article: Key points for high-mobility organic field-effect transistors. *Adv. Mater.* **25**, 6158-6183 (2013).

5 Noriega, R. *et al.* A general relationship between disorder, aggregation and charge transport in conjugated polymers. *Nat. Mater.* **12**, 1038-1044 (2013).

6 Wang, C. *et al.* High dielectric constant semiconducting poly(3-alkylthiophene)s from side chain modification with polar sulfinyl and sulfonyl groups. *Macromolecules* **51**, 9368-9381 (2018).

7 Green, M. A., Ho-Baillie, A. & Snaith, H. J. The emergence of perovskite solar cells. *Nat. Photonics* **8**, 506-514 (2014).

8 Wang, S. *et al.* Band-like transport in surface-functionalized highly solution-processable graphene nanosheets. *Adv. Mater.* **20**, 3440-3446 (2008).

9 Wannier, G. H. Dynamics of band electrons in electric and magnetic fields. *Rev.Mod. Phys.* **34**, 645-655 (1962).

10 Gregory, D. S. & Rumbles, G. Excitons in nanoscale systems. *Nat. Mater*. **5**, 683-696 (2006).

11 Hartley, C. S., Elliott, E. L. & Moore, J. S. Covalent assembly of molecular ladders. *J. Am. Chem. Soc.* **129**, 4512-4513 (2007).
12 Venkateshvaran, D. *et al.* Approaching disorder-free transport in high-mobility conjugated polymers. *Nature* **515**, 384-388 (2014).
13 Jin, X.-H. *et al.* Long-range exciton transport in conjugated polymer nanofibers prepared by seeded growth. *Science* **360**, 897-900 (2018).
14 Haedler, A. T. *et al.* Long-range energy transport in single supramolecular nanofibres at room temperature. *Nature* **523**, 196-199 (2015).
15 Xu, B. *et al.* Donor conjugated polymers with polar side chain groups: The role of dielectric constant and energetic disorder on photovoltaic performance. *Adv. Funct. Mater.* **28**, 1803418 (2018).
16 Torabi, S. *et al.* Strategy for enhancing the dielectric constant of organic semiconductors without sacrificing charge carrier mobility and solubility. *Adv. Funct. Mater.* **25**, 150-157 (2015).
17 Xie, X. *et al.* Nanogridarene: A rising nanomolecular integration platform of organic intelligence. *Chin. J. Chem.* **38**, 103-105 (2020).
18 Ruffieux, P. *et al.* On-surface synthesis of graphene nanoribbons with zigzag edge topology. *Nature* **531**, 489-492 (2016).
19 Schlüter, A.-D. Ladder Polymers: The new generation. *Adv. Mater.* **3**, 282-291 (1991).
20 Goldfinger, M. B. & Swager, T. M. Fused polycyclic aromatics via electrophile-induced cyclization reactions: Application to the synthesis of graphite ribbons. *J. Am. Chem. Soc.* **116**, 7895-7896 (1994).
21 Sedghi, G. *et al.* Comparison of the conductance of three types of porphyrin-based molecular wires: *β*,meso,*β*-fused tapes, meso-butadiyne-linked and twisted meso-meso linked oligomers. *Adv. Mater.* **24**, 653-657 (2012).
22 Ikai, T. *et al.* Triptycene-based ladder polymers with one-handed helical geometry. *J. Am. Chem. Soc.* **141**, 4696-4703 (2019).
23 Kim, F. S., Ren, G. & Jenekhe, S. A. One-dimensional nanostructures of π-conjugated molecular systems: Assembly, properties, and applications from photovoltaics, sensors, and nanophotonics to nanoelectronics. *Chem. Mater.* **23**, 682-732 (2011).
24 Feng, Q. Y. *et al.* A robust and soluble nanopolymer based on molecular grid-based nanomonomer. *Chin. J. Polym. Sci.* **35**, 87-97 (2017).
25 Lin, D. *et al.* Stereoselective gridization and polygridization with centrosymmetric molecular packing. *Nat. Commun.* **11**, 1756 (2020).
26 Heeger, A. J. Semiconducting polymers: The third generation. *Chem. Soc. Rev.* **39**, 2354-2371 (2010).
27 Gettinger, C. L., Heeger, A. J., Drake, J. M. & Pine, D. J. A photoluminescence study of poly(phenylene vinylene) derivatives: The effect of intrinsic persistence length. *J. Chem. Phys.* **101**, 1673-1678 (1994).
28 Yashima, E., Maeda, K. & Furusho, Y. Single- and double-stranded helical polymers: Synthesis, structures, and functions. *Acc. Chem. Res.* **41**, 1166-1180 (2008).
29 Wang, L. *et al.* Friedel–Crafts bottom-up synthesis of fluorene-based soluble luminescent organic nanogrids. *Org. Lett.* **16**, 1748-1751 (2014).

30 Bustamante, C., Marko, J. F., Siggia, E. D. & Smith, S. Entropic elasticity of lambda-phage DNA. *Science* **265**, 1599-1600 (1994).
31 Xie, L. H. *et al.* Facile synthesis of complicated 9,9-diarylfluorenes based on $BF_3 \cdot Et_2O$-mediated Friedel−Crafts reaction. *Org. Lett.* **8**, 3701-3704 (2006).
32 Nagai, M., Huang, J., Zhou, T. & Huang, W. Effect of molecular weight on conformational characteristics of poly(3-hexyl thiophene). *J. Polym. Sci. Part B-Polym. Phys.* **55**, 1273-1277 (2017).
33 Mertens, H. D. T. & Svergun, D. I. Structural characterization of proteins and complexes using small-angle X-ray solution scattering. *J. Struct. Biol.* **172**, 128-141 (2010).
34 Cotts, P. M., Swager, T. M. & Zhou, Q. Equilibrium flexibility of a rigid linear conjugated polymer. *Macromolecules* **29**, 7323-7328 (1996).
35 Chen, J. H. *et al.* Gelation and its effect on the photophysical behavior of poly(9,9-dioctylfluorene-2,7-diyl) in toluene. *Macromolecules* **42**, 1306-1314 (2009).
36 Trilling, F., Ausländer, M.-K. & Scherf, U. Ladder-type polymers and ladder-type polyelectrolytes with on-chain dibenz[a,h]anthracene chromophores. *Macromolecules* **52**, 3115-3122 (2019).
37 Pei, Q. & Yang. Efficient photoluminescence and electroluminescence from a soluble polyfluorene. *J. Am. Chem. Soc.* **118**, 7416-7417 (1996).
38 Scherf, U. & List, E. J. W. Semiconducting polyfluorenes—towards reliable structure–property relationships. *Adv. Mater.* **14**, 477-487 (2002).
39 Ton-That, C., Weston, L. & Phillips, M. R. Characteristics of point defects in the green luminescence from Zn- and O-rich ZnO. *Phys. Rev. B* **86**, 115205 (2012).
40 Connell, M. J. *et al.* Band gap fluorescence from individual single-walled carbon nanotubes. *Science* **297**, 593-596 (2002).
41 Tabor, D. P. *et al.* Design rules for high mobility xanthene-based hole transport materials. *Chem. Sci.* **10**, 8360-8366 (2019).
42 Mozer, A. J. *et al.* Charge carrier mobility in regioregular poly(3-hexylthiophene) probed by transient conductivity techniques: A comparative study. *Phys. Rev. B* **71**, 035214 (2005).
43 Blakesley, J. C. *et al*. Temperature-dependent electron and hole transport in disordered semiconducting polymers: Analysis of energetic disorder. *Phys. Rev. B* **81**, 045210 (2010).
44 Liu, B. *et al.* A highly crystalline and wide-bandgap polydiarylfluorene with *β*-phase conformation toward stable electroluminescence and dual amplified spontaneous emission. *ACS Appl. Mater. Interfaces* **8**, 21648-21655 (2016).
45 Yin, H. *et al.* Thick-film high-performance bulk-heterojunction solar cells retaining 90% PCEs of the optimized thin film cells. *Adv. Electron. Mater.* **3**, 1700007 (2017).
46 Abbaszadeh, D. *et al.* Elimination of charge carrier trapping in diluted semiconductors. *Nat. Mater.* **15**, 628-633 (2016).
47 Yang, L. *et al.* A novel structure of grid spirofluorene: a new organic semiconductor with low reorganization energy. *New J. Chem.* **43**, 7790-7796 (2019).

48 Wang, J. *et al.* Variable polymer properties driven by substituent groups: Investigation on a trifluorovinylether-functionalized polyfluorene at the C-9 position. *Macromol. Chem. Phys.* **216**, 742-748 (2015).
49 Shao, P. *et al.* Flexible films of covalent organic frameworks with ultralow dielectric constants under high humidity. *Angew. Chem. Int. Ed.* **57**, 16501-16505 (2018).
50 Brebels, J. *et al*. High dielectric constant conjugated materials for organic photovoltaics. *J. Mater. Chem. A* **5**, 24037-24050 (2017).
51 Morawska, P. O. *et al.* Side-chain influence on the mass density and refractive index of polyfluorenes and star-shaped oligofluorene truxenes. *J. Phys. Chem. C* **119**, 22102-22107 (2015).
52 Boufflet, P. *et al.* The influence of backbone fluorination on the dielectric constant of conjugated polythiophenes. *Adv. Electron. Mater.* **4**, 1700375 (2018).
53 Donaghey, J. E. *et al*. Dielectric constant enhancement of non-fullerene acceptors via side-chain modification. *Chem. Commun.* **51**, 14115-14118 (2015).
54 Sun, L. *et al*. Structure-induced high dielectric constant and low loss of CNF/PVDF composites with heterogeneous CNF distribution. *Nanotechnology* **21**, 305702 (2010).

Acknowledgments: We thank Shanghai Synchrotron Radiation Facility (SSRF) to provide synchrotron radiation SAXS instruments (BL19U2). We thank daxia Xia and Haowan Cheng from Shiyanjia Lab (www.Shiyanjia.com) for the simulation of the vibrational modes and the molecular orbital distribution, as well as providing the ellipsometry measurements. **Funding:** This work was supported by the National Natural Science Foundation of China (21774061, 22071112 and 61935017), Natural Science Foundation major research program integration project (Grant Number 91833306), Six Peak Talents Foundation of Jiangsu Province (XCLCXTD-009), Open Project from State Key Laboratory of Supramolecular Structure and Materials at Jilin University (No. sklssm202014).

Author contributions: Dongqing Lin has written this manuscript and Supplementary Materials, performed polygridization, simulated conformational relaxations, analysized single-chain and optoelectronic properties. Wenhua Zhang has provide SAXS characterizations. Yongxia Yan, Hongkai Hu and Lei Tang have synthesized the substrates of NPSG. Hang Yin and Haixia Hu have measured and calculated the carrier mobility. Haifeng Ling and Le Wang have measured and calculated the dielectric constant. Xingmiao Xie and Xuefeng Guo have fabricated the single-molecular electronic device to measure the conductance of NPSG. Dan Lu and Hao Zhang have provided SLS characterizations. Ying Wei has provided significant suggestions on the synthesis of NPSG, and carefully checked this manuscript and Supplementary Materials. Zhang He, Shasha Wang, Jin'an Liu and Que Qian have provided crucial help in nanotechnological and photophysical characterizations. Yongxia Wang and Chaoyang Dong have helped to address the figures. Linghai Xie and Wei Huang has initiated this project, provided crucial idea and offers enough funds for this work;

Data and materials availability: All data is available in the main text or the supplementary Informations. The data are available from the corresponding author on reasonable request.

Competing interests: Authors declare no competing interests;